J. Phys. B: At. Mol. Opt. Phys. 24 (1991) 1557–1574. Printed in the UK

The even-parity $J = 0$ autoionizing spectrum of strontium below the $4d_{5/2}$ threshold: observation and theoretical analysis

M Kompitsas†, S Goutis†, M Aymar‡ and P Camus‡

† Theoretical and Physical Chemistry Institute, National Hellenic Research Foundation, 48, Vasileos Constantinou Avenue, Athens 11635, Greece

‡ Laboratoire Aimé Cotton, Centre National de la Recherche Scientifique, Batiment 505, Campus d'Orsay, 91405 Orsay Cedex, France

Received 28 November 1990

Abstract. The even parity $J = 0$, 1 and 2 autoionizing spectra of Sr have been observed below the $4d_{5/2}$ threshold using two-step laser spectroscopy from the ground state atom $5s^2$ in an atomic beam.

Resonant excitations of the autoionizing states are observed by time-of-flight (TOF) analysis of the produced ions. In this experiment via the $4d5p\ ^1P_1$ intermediate level, the $J = 0$ resonances are selectively identified among the other $J = 1$ or 2 ones by comparing the line intensities from two spectra recorded with $\pi\pi$ and $\pi\sigma$ polarizations of the two laser beams.

From the $J = 0$ data, the $J = 0$ $4d_{3/2}nd_{3/2}$ and $4d_{5/2}nd_{5/2}$ series are observed up to $n = 66$ and 64 respectively. In addition we also observed the $5p^2\ ^1S_0$ level, whose location has been controversial for a long time: this level is now identified with a broad autoionizing resonance at $54\,451 \pm 30\ cm^{-1}$. It has also been observed in this work by a direct two-photon excitation.

It is shown that the $4dnd$ series are strongly perturbed by the $5p^2\ ^1S_0$ level and also by the $5p6p\ ^3P_0$ level which has not yet been observed experimentally. The experimental data are successfully interpreted using a theoretical approach which combines the eigenchannel R-matrix and multichannel quantum defect methods.

1. Introduction

The development of various multistep and multiphoton laser techniques during recent years has resulted in an increased number of detailed experimental data on autoionizing doubly excited states of the alkaline-earth atoms. This paper deals with the autoionizing spectrum of Sr, which has been much less studied than Ba in laser experiments because of its higher ionization limit.

Most of the previous experimental investigations on the autoionizing spectrum of Sr deal with the odd parity states. Spectroscopic data on the $J = 1$ levels have been obtained by standard UV absorption spectroscopy from the $5s^2\ ^1S_0$ ground state (Garton and Codling 1968, Hudson *et al* 1969, Connerade *et al* 1980, Brown *et al* 1983). Emission spectroscopy from an arc has been performed by Newsom *et al* (1973) and few low-lying autoionizing levels have been observed. Extensions of the observations to other J values have been performed by using multistep laser spectroscopy (Xu *et al* 1986, 1987, Zhu *et al* 1987, Kompitsas *et al* 1990).

0953-4075/91/071557+18$03.50

On the theoretical side, several works have demonstrated recently that a good description of doubly excited states of alkaline earths can be obtained by combining the eigenchannel R-matrix method, developed by Greene (1985) with the multichannel quantum defect theory (MQDT) (Seaton 1983, Fano and Rau 1986). This approach has been successfully employed in Sr to analyse energy level positions, autoionization profiles (Aymar *et al* 1987, Aymar 1987, Kompitsas *et al* 1990) and photoelectron spectra (Aymar and Lecomte 1989).

Concerning the even-parity spectrum of Sr, the $^1S_0$ and $^1D_2$ spectra were investigated but the above-threshold experimental data were too scarce to allow the reliability of the predicted energies to be tested. The purpose of this paper is to deliver new experimental data on the even-parity autoionizing $J=0$ spectrum of Sr. Investigation of this spectrum is of particular interest because controversies arose over where the $5p^2\,^1S_0$ level lies. The $5p^2\,^1S_0$ label was initially given to the level at 37 160.28 cm^{-1} in Moore's table (1971). However this assignment has been questioned in multiconfiguration Hartree–Fock (Froese-Fischer and Hansen 1981, Aspect *et al* 1984) and R-matrix (Aymar *et al* 1987) calculations, giving a dominant $4d^2$ character to that energy level and predicting the location (Aymar *et al* 1987) of the $5p^2\,^1S_0$ above the ionization limit. One motivation of the present work is to check this prediction.

We report in this paper new experimental data on the even-parity $J=0$ spectrum obtained using two-step laser excitation techniques. In this experiment, the autoionizing spectrum has been recorded via the $4d5p\,^1P_1$ intermediate level. The $J=0$ levels are identified among the possible $J=0$, 1, 2 resonances by comparing two different records with $\pi\pi$ and $\pi\sigma$ linear polarization for the two lasers. Observed data mainly concern the two $4d_{3/2}nd_{3/2}$ and $4d_{5/2}nd_{5/2}$ $J=0$ series. In addition an important result of our investigation is the observation of the $5p^2\,^1S_0$ level above the first ionization limit which is identified with a broad $J=0$ autoionizing resonance at $54\,451\pm30$ cm^{-1}. Data on the even parity $J=1$ and $J=2$ spectra are currently under analysis and will be given in a forthcoming paper.

The interpretation of the experimental data is performed by a theoretical approach combining the eigenchannel R-matrix and MQDT methods. This approach provides a very good description of the energy of the observed members of the $4dnd$ $J=0$ series which are strongly perturbed as expected by the newly observed $5p^2\,^1S_0$ level but also by the predicted $5p6p\,^3P_0$ level which has not been observed yet.

2. Experimental set-up

The detailed description of the apparatus (see figure 1), has been given elsewhere (Kompitsas *et al* 1990). Briefly, a Sr effusive atomic beam is produced in a resistively heated oven. Following the two-step laser photoionization, the Sr ions produced are detected in a homemade time-of-flight mass spectrometer and the signal is processed by usual boxcar techniques and recorded simultaneously on a chart recorder and a computer.

The even autoionizing spectrum lying in the 54 000–60 800 cm^{-1} region is excited from the ground state by a two-step process. In this kind of experiment the spectra are dependent on the low jitter of the two synchronized pump beams. Thus an electronic circuit (at a repetition rate of 10 Hz) is developed which fires the lasers, controls the pulses to the mass spectrometer and triggers the signal processing. The electronic

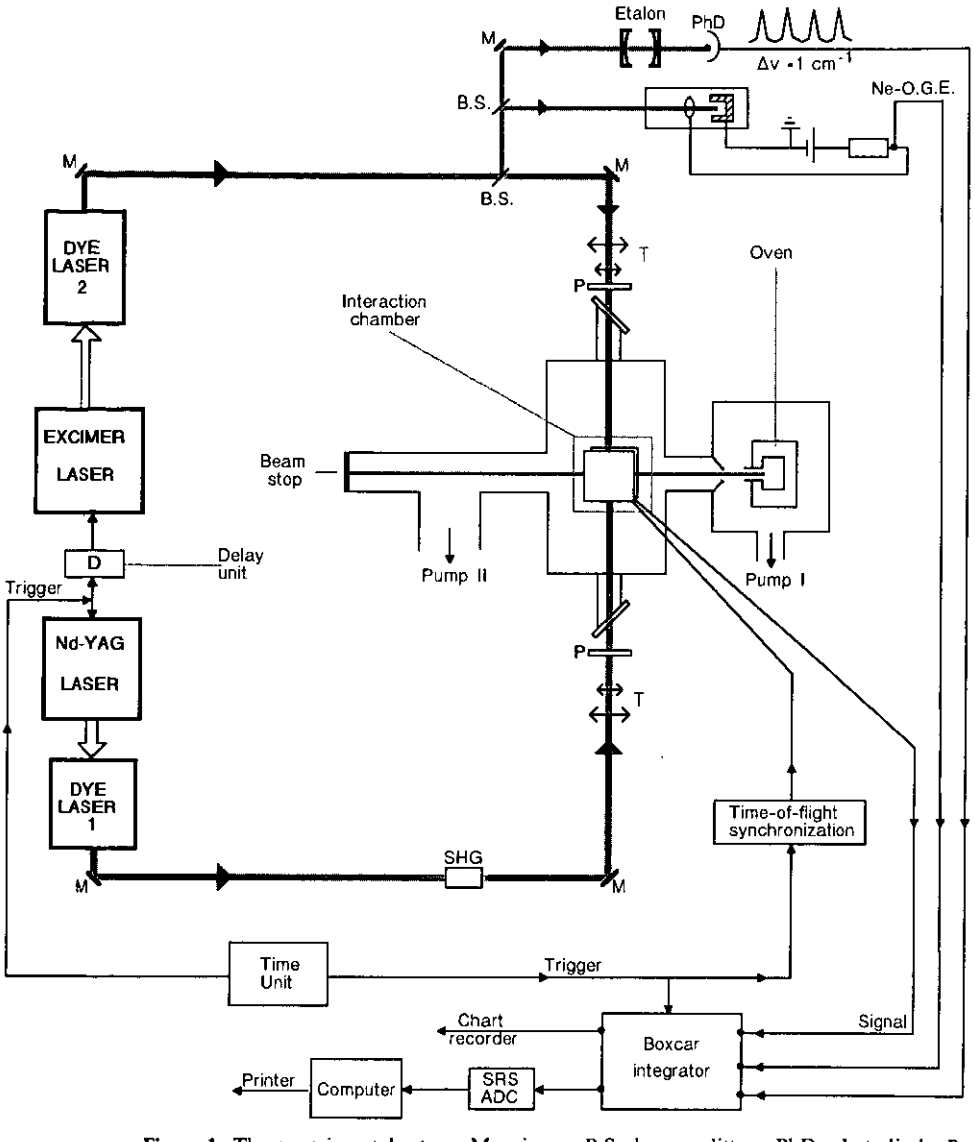

Figure 1. The experimental set-up. M: mirrors, B.S.: beam splitters, PhD: photodiode, P: polarizer, T: telescope, SHG: second harmonic generation crystal.

synchronization of the two pump lasers allows an adjustable delay within a few ns which is crucial for the signal-to-noise ratio of the recorded spectra.

The first-step laser system (called UV laser hereafter) consisted of a Nd-YAG-pumped dye laser (Datachrom from Quantel). The Coumarin 480 dye output (around 5 mJ/pulse energy) is frequency doubled in a LFM crystal (Quantum Tecnology) which delivers about 100 μJ of UV light in the 240-260 nm range. This laser beam is used to populate selectively appropriate $^1P_1$ odd intermediate states. The second-step laser was an excimer pumped dye laser tuned in the 500-680 nm region to excite the final autoionizing state. This system (called visible) is counterpropagating along the first one. The two unfocused beams cross perpendicularly the atomic beam and are linearly polarized

by Glan–Thomson prisms placed just before the vacuum chamber entrance windows. The relative direction of the linear polarizations of the two beams is experimentally adjusted in a known two-step resonance. The linewidth of the second laser is about 0.2 cm^{-1} and its wavelength is calibrated by simultaneously recording a Ne-optogalvanic spectrum and the transmission fringes of a 1 cm^{-1} free-spectral-range Fabry–Perot interferometer. The pulse energy is varied between 3 and 10 μJ by neutral glass filters so that line broadening could be avoided.

3. Two-step experiment and *J*-selection rules using polarization spectroscopy

During most of these measurements, the UV laser excites the level positioned at 41 172.15 cm^{-1} ($\lambda = 242.9$ nm). It is labelled in Moore's table (1971) as 5s8p $^1P_1$. Other reports (Garton and Codling 1968, Baig and Connerade 1984) proposed the 4d5p $^1P_1$ label for this level. Then it was confirmed by many calculations done with the empirical MQDT (Lu 1977, Esherick 1977), the MCHF method (Vaeck *et al* 1988) or the *R*-matrix method (Aymar *et al* 1987). All these calculations showed that the 4d5p character is spread out in many 5s*n*p $^1P_1$ levels with the maximum value in the level at 41 172.15 cm^{-1}. We used therefore this intermediate level since a large oscillator strength for the second step transition to the $5p^2$ and 4d*n*d states is expected. This fact accounted for the best signal-to-noise ratio for the 41 172.15 cm^{-1} level when probing the other surrounding 5s*n*p $^1P_1$ intermediate states.

Starting from the Sr ground state with a zero total angular momentum, one can detect in a two-step excitation process as described above 17 Rydberg series 4d*nl* with $l = 0, 2, 4$ with J equal to 0, 1 or 2 and the expected $5p^2$ $J = 0$ resonance. There are only two 4d*n*d series for $J = 0$ angular momentum to be observed here. We apply therefore the two-step polarization technique from the intermediate 41 172.15 cm^{-1} $J = 1$ level which enables us to identify the $J = 0$ states among transitions corresponding to $J = 0, 1, 2$ final states.

This intermediate level is always excited by π light so that only the $J = 1$, $m_J = 0$ sublevel is populated. The method applies then under the condition that it does not depolarize before absorption of the second photon. The collisions in the atomic beam and radiative decay followed by reabsorption of a resonant photon by a ground-state atom (radiation trapping) can be regarded as possible depolarization mechanisms. Both processes can be neglected here due to the low density of Sr atoms in the interaction region which is about 10^9 atoms/cm^3.

More critical appeared to be the partial depopulation of the 4d5p $^1P_1$ level by radiation to lower levels. Its lifetime is of the order of 27 ns (Jonsson *et al* 1984) which is almost twice the laser pulse duration. In this case subsequent absorption of a visible photon gives weak lines due to this mechanism and they have been observed to overlap the spectrum. We have assigned all these lines to transitions to the odd autoionizing levels (Kompitsas *et al* 1990). At a given pulse energy of the second laser, by adjusting electronically the delay within the ns range between the two lasers we can mostly eliminate such parasitic lines.

According to the relative orientation of the polarization of the second laser we can distinguish the following two cases.

(*a*) The second laser is linearly polarized into the same direction as the first one ('$\pi\pi$ position'), then the final sublevel can be $J = 0$ and $m_J = 0$ or $J = 2$ and $m_J = 0$.

Figure 2(*b*) shows a typical $\pi\pi$ spectrum where only transitions to upper levels with $J=0$ and 2 are enhanced.

(*b*) The second laser is linearly polarized perpendicularly to the direction of the first one ('$\pi\sigma$ position'). Applying again the selection rules $\Delta m_J = \pm 1$ for the second step transition it follows that the final sublevel can be $J=1$ and $m_J = \pm 1$ or $J=2$ and $m_J = \pm 1$. Figure 2(*c*) shows a typical $\pi\sigma$ spectrum in the same spectral region as in figure 2(*b*).

So by comparing the line intensities in the two $\pi\pi$ and $\pi\sigma$ spectra recorded in the same energy range we are able to distinguish $J=0$ upper levels whose transitions appear only on $\pi\pi$ spectra and $J=1$ upper levels which appear only on $\pi\sigma$ spectra.

How effectively the polarization method works depends again on the intensity of the visible laser and how carefully the relative direction of the two polarizations can be realized. We present some general observations and use slightly different experimental conditions in different energy regions to identify the J values. (*a*) The transitions leading to the $4d_{5/2}nd$ $J=0$ series are always stronger than the ones to the $4d_{3/2}nd$ $J=0$ series. In the lower part of the spectrum (54 000–59 500 cm^{-1}) with a visible laser energy of 3–6 μJ, the unfavoured $4d_{3/2}nd$ $J=0$ lines in the $\pi\sigma$ spectra are totally eliminated while only few weak lines pertaining to $4d_{5/2}nd$ $J=0$ are observed. (*b*) Most of the $J=2$ transitions are weaker than the $J=0$ ones, so in the higher part of the spectra the laser intensity can be increased to 10–12 μJ to obtain enough intensity of the $J=2$ transitions which serve also as secondary standards in all spectra. (*c*) Finally in this higher intensity condition when the $J=0$ lines appear in the $\pi\sigma$ position as small peaks, they are always increased by an order of magnitude in the $\pi\pi$ spectra. Similar observations are made concerning the $J=1$ resonances. To conclude, the J assignment by comparing $\pi\pi$ and $\pi\sigma$ spectra is effective for most of the observed transitions.

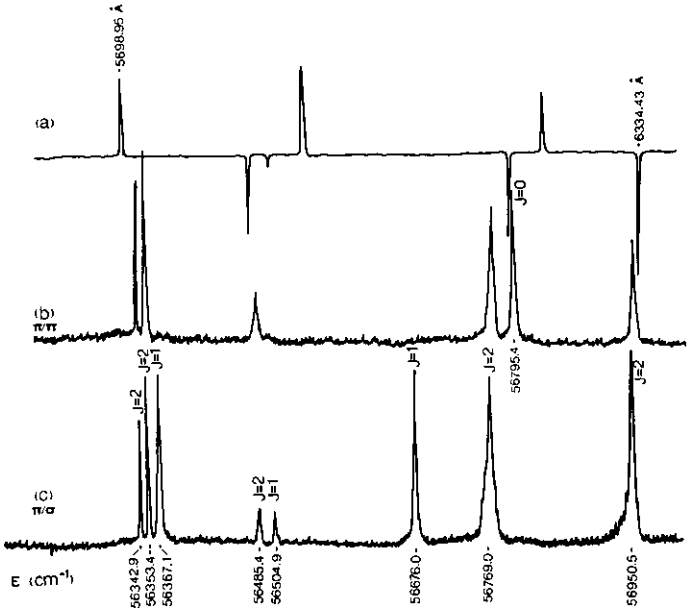

Figure 2. (*a*) Ne optogalvanic spectrum. (*b*) $\pi\pi$ spectrum, only resonances corresponding to $J=0$ or 2 appear. (*c*) $\pi\sigma$ spectrum, only resonances corresponding to $J=1$ or 2 appear.

4. Measurements and results

4.1. $5p^2\ ^1S_0$ and low-lying 4d6d ($n = 4, 5$) $J = 0$ levels

The lowest members $n = 5, 6$ of the 4d*n*d series and the expected $5p^2\ ^1S_0$ level are placed energetically such that they can also be excited in the direct two-photon process. Newsom *et al* (1973) identified the 4d5d $J = 1$ and $J = 2$ states in the 49 200–51 600 cm^{-1} range and the 4d6d $^3F_2$ state at 54 891.3 cm^{-1}. We use the set-up of section 2 operating it with only one focused dye laser beam with its wavelength in the 350–407 nm range. Following similar arguments to those exposed in section 3 we can induce transitions to final states with $J = 0$ and 2 by a linearly polarized beam and to states with $J = 2$ by a circularly polarized beam. In the following we can summarize our results.

(*a*) Three resonances of the Fano type are observed corresponding to the 4d5d configuration, previously observed by Newsom, at 51 036 cm^{-1} ($^3F_2$), 51 356 cm^{-1} ($^1D_2$) and 51 555 cm^{-1} ($^3P_2$) energy positions. There is no evidence for the two 4d5d $J = 0$ levels, which are also missing in Newsom's results from emission spectra. We assume that they are broad and very weak when excited directly from the ground state.

(*b*) Lines corresponding to the $J = 0$ and 2 low member 4d6d are presented for the first time in figure 3. The five narrow lines are identified with 4d6d $J = 0$ and $J = 2$ levels; among these levels only the $^3F_2$ was previously observed by Newsom *et al* (1973). The additional 5d6d $^3D_2$ level is expected to lie outside the energy range considered here, at lower energy. The broad asymmetric structure is then attributed to the $5p^2\ ^1S_0$ level.

(*c*) The differences between the linear and circular polarization rules in the amplitude of the $J = 0$ transitions are not so pronounced as expected, thus limiting the J assignment of the final level. This may be due either to a partial destruction of the selected polarization by focusing the laser beam as previously observed (Camus *et al* 1989) or to a not perfectly circular polarization when scanning the dye laser over a large region. So we are not using this two-photon excitation scheme further.

To verify the above observations and for accurate energy level determination we have applied the two-step method via the intermediate 5s7p $^1P_1$ level at 38 910 cm^{-1}. Figure 4 gives a part of this $\pi\pi$ spectrum. The broad structure assigned to a $J = 0$ final level is the $5p^2\ ^1S_0$ autoionizing resonance previously observed in the two-photon experiment. Its energy value is given at 54 451 ± 30 cm^{-1}.

Oscillator strength using the 4d5p $^1P_1$ intermediate state in the two-step experiment would probably be larger than in the previous study using the 5s7p intermediate. But the wavelength of the second-step laser is then too far in the red to be pumped by an excimer laser.

4.2. Upper members of the 4dnd $J = 0$ series

Figure 5 shows a part of the Sr spectrum which lies between the 5s and the 5p thresholds, relevant for this experiment. Also shown are the lowest members $4d^2$ $J = 0$ and the $5p^2\ ^3P_0$ (Moore 1971) which are bound. We adopt the $4d^2\ ^1S_0$ assignment for the level at 37 160.28 cm^{-1} (in Moore's table it is labelled as $5p^2\ ^1S_0$) since according to Aymar *et al* (1987) it has twice as much $4d^2$ character as $5p^2$. In this study we find that the $5p^2\ ^1S_0$ is above the first ionization limit and located at 54 451 cm^{-1}. Following the two step polarization method described above we have observed the 4d*n*d $J = 0$ series ($n \geqslant 7$) up to the $4d_{5/2}$ threshold and the results are given in table 1.

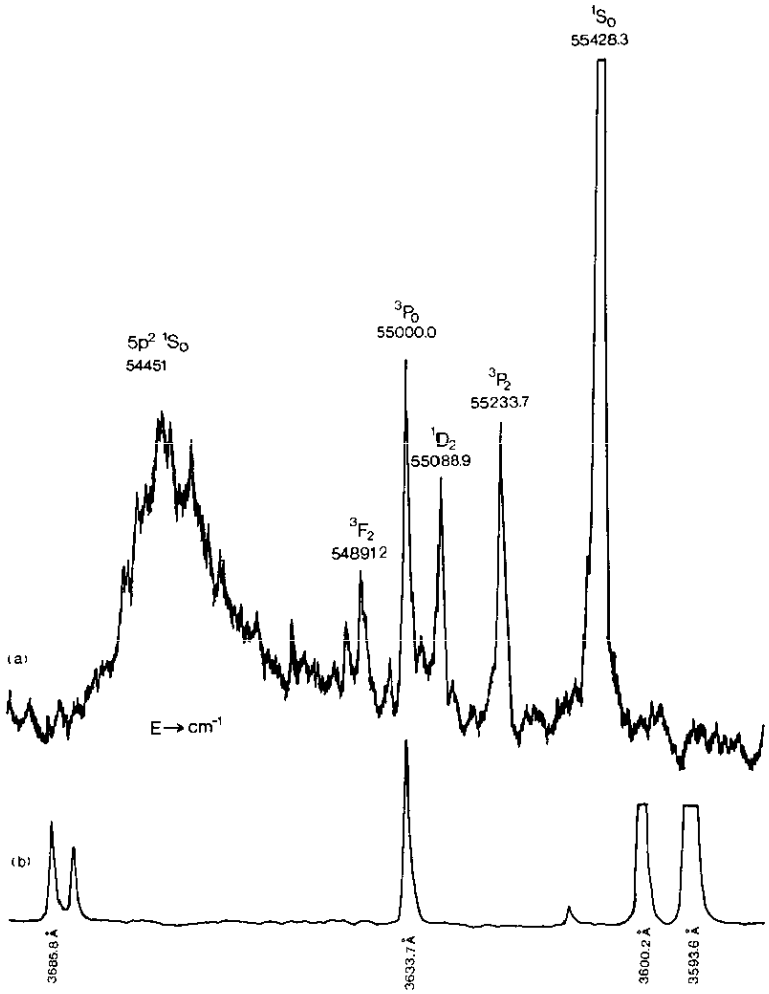

Figure 3. (*a*) Two-photon direct excitation of the $5p^2\ ^1S_0$ level and some $J=0$ and 2 members of the 4d6d configuration. (*b*) Ne optogalvanic spectrum.

We estimate now the accuracy of the given values of the energy positions and widths presented in table 1. In almost all the cases the $J=0$ levels are isolated resonances and their positions (peak value) have been measured to an accuracy of 0.3 cm^{-1}: this results from the linewidth of the second step laser and from the laser wavelength calibration accuracy (optogalvanic standard reference and etalon fringes). The effect of the width of the short-lived intermediate level ($\Delta E = 6$ MHz) can be neglected. The standard deviation of the averaged results obtained from two independent measurements is 0.2 cm^{-1} or less. There are a few cases where the $J=0$ and 2 resonances partially blend each other. But since their widths are less than 2 cm^{-1} their peak positions can be unambiguously determined with a similar accuracy as above. On the other hand, less accurate in such cases is the determination of the width of the two resonances and their approximated values are given in table 1 denoted by B. For the broad lines, as mainly observed in the lower part of the spectrum, we estimate an energy value accuracy of one tenth of the line width.

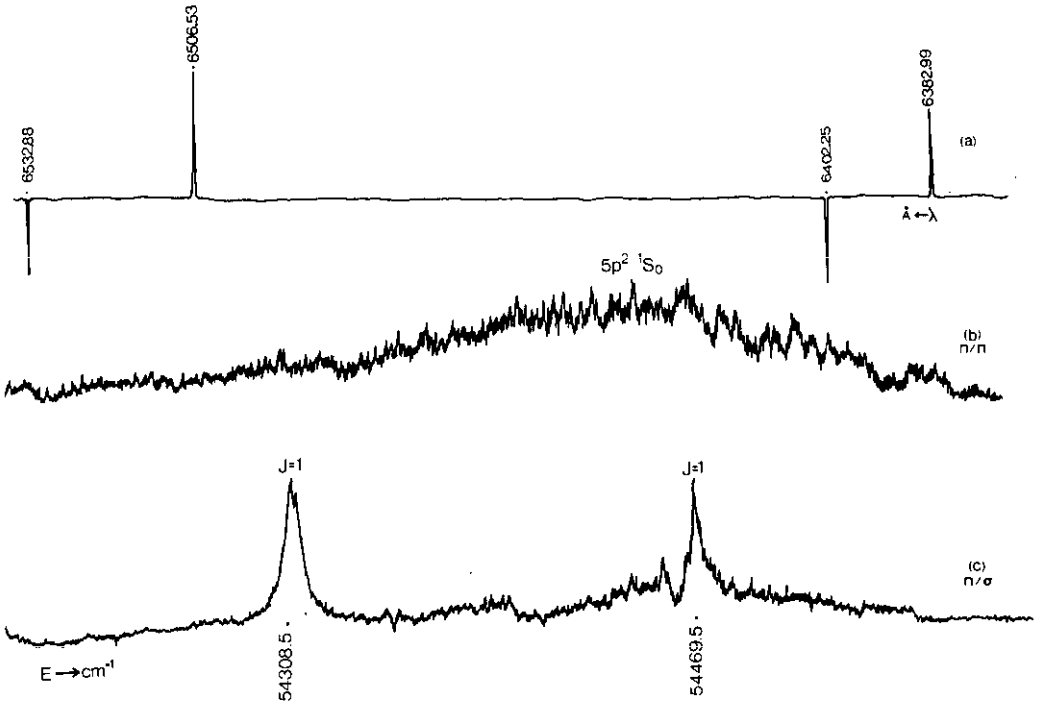

Figure 4. (*a*) Ne optogalvanic spectrum. Two-step excitation of the $5p^2\ ^1S_0$ level: (*b*) $\pi\pi$ spectrum, $J=0$ or 2 is favoured. (*c*) $\pi\sigma$ spectrum, $J=1$ or 2 is favoured. The $J=1$ resonances belong to the 4d6d configuration.

In figure 6 the region 59 000–59 400 cm^{-1} is shown in detail, where, according to the theoretical predictions (see sections 5.2 and 5.3), the second perturber $5p6p\ ^3P_0$ of the $J=0^e$ series should lie. Its predicted position (59 065 cm^{-1}) is marked by an arrow (A) while the arrow (B) indicates the predicted position (59 323 cm^{-1}) of the perturbed $4d_{3/2}11d$ $J=0$ level. By comparing $\pi\pi$ and $\pi\sigma$ spectra there is no evidence of both levels even though the spectrum is recorded with a high sensitivity of the detection system to identify possible weak transitions at the predicted positions. The weak $J=1$ transitions in the $\pi\sigma$ spectra appear due to the high sensitivity of the detector. On the other hand we have recorded the strong $4d_{5/2}10d$ resonance at 59 258.8 cm^{-1}.

In figure 7 the $\pi\pi$ and $\pi\sigma$ spectra are compared to show the decreasing intensity of the $4d_{3/2}nd$ $J=0$ series. On the other hand the intensities of the series members $4d_{5/2}nd$ with $n=19$ to 21 are considerably stronger. In this energy range, close to the $4d_{3/2}$ limit, the $4d_{3/2}nd$ series members mix with low members of the series converging to the $4d_{5/2}$ limit. The former are also being overlapped by $J=2$ resonances converging towards the same $4d_{3/2}$ limit. Due to these reasons and to the lack of resolution of our experimental set-up we have not been able to measure the positions of the $J=0$ $4d_{3/2}nd$ resonances above $n=64$.

5. Theoretical analysis

5.1. General procedure

The analysis of the experimental data has been performed by combining the eigenchan-

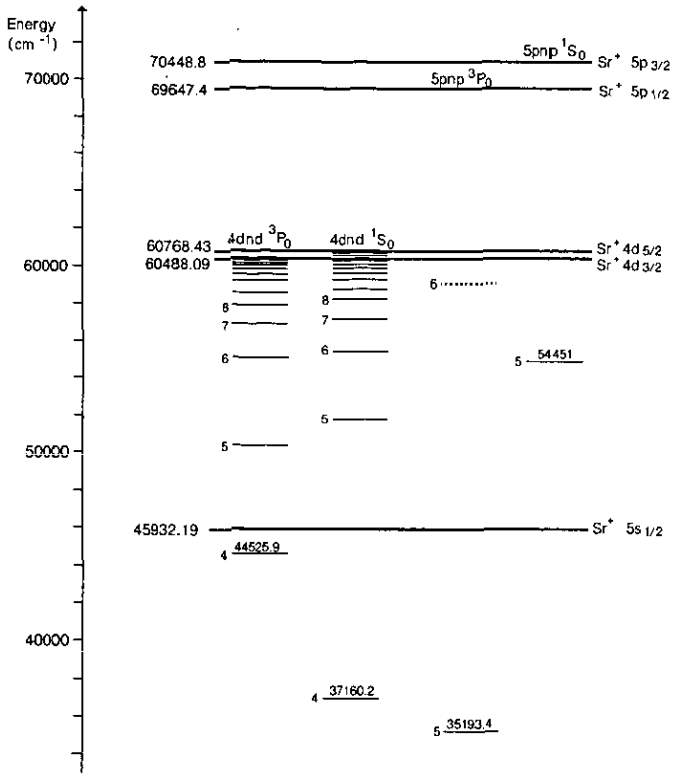

Figure 5. Part of the Sr energy diagram relevant in this experiment.

nel R-matrix and MQDT methods. The calculations proceed along the same lines as those previously done to describe doubly excited states of Ca (Kim and Greene 1987, 1988), Sr (Aymar 1987, Kompitsas *et al* 1990) and Ba (Aymar 1990).

Briefly, the eigenchannel R-matrix (Greene 1985) is used to variationally determine the LS-coupled wavefunctions of the valence electron pair within a finite reaction volume. We use a reaction volume of radius $r_0 = 20$ au. The two-electron basis functions are antisymmetrized products of one-electron orbitals coupled to form definite orbital and spin angular momenta. The one-electron orbitals are numerical eigenfunctions of the e-Sr^{2+} Schrödinger equation. The form of the e-Sr^{2+} potential used in this work is similar to the e-Ba^{2+} potential of Aymar (1990). It includes a screening term and a polarization term, both terms being l-dependent,

$$U(r) = -\frac{1}{r}[2+36\exp(-\alpha_1^l r)+\alpha_2^l r\exp(-\alpha_3^l r)]-\frac{\alpha_d}{2r^4}\left\{1-\exp\left[-\left(\frac{r}{r_c^l}\right)^6\right]\right\}.$$

The dipole polarizability α_d of the Sr^{2+} ion is fixed to 7.4 au and the empirical parameters α_1^l and r_c^l are adjusted to give accurate energy levels of the Sr^+ spectrum.

Two independent R-matrix calculations are done for the $^1S^e$ and $^3P^e$ symmetries; they involve the $5s\varepsilon s$, $4dnd$, $5pnp\ ^1S^e$ and $4dnd$, $5pnp\ ^3P^e$ channels respectively. The R-matrix calculations give the logarithmic derivatives of the escaping electron's wavefunction at the reaction surface which are converted into smooth LS-coupled short-range reaction matrices. These matrices are determined as explicit functions of

Table 1. List of energy levels, widths and quantum defects of the even $J=0$ autoionizing states of Sr below the $4d_{5/2}$ limits. Comparison with theory. (NO: not observed, B: blended with a $J=2$ level, †: observed via the 5s7p intermediate level, ‡: tentatively assigned).

$E_{expt.}$ (cm^{-1})	Width (cm^{-1})	$\nu d_{3/2}$	$\nu d_{5/2}$	$E_{theor.}$ (cm^{-1})	Label
NO	—	—	—	50 975	$4d_{3/2}5d$
NO	—	—	—	51 681	$4d_{5/2}5d$
54 451.0†	230.0	4.26	4.17	54 597	$5p^2\,{}^1S_0$
54 999.9†	4.0	4.47	4.36	54 965	$4d_{3/2}6d$
55 428.3†	2.0	4.66	4.53	55 398	$4d_{5/2}6d$
56 795.4	8.0	5.45	5.26	56 792	$4d_{3/2}7d$
57 142.9	28.0	5.73	5.50	57 127	$4d_{5/2}7d$
57 844.2	1.5	6.44	6.13	57 825	$4d_{3/2}8d$
58 154.8	8.0	6.86	6.48	58 143	$4d_{5/2}8d$
58 431.1	3.8	7.30	6.85	58 457	$4d_{3/2}9d$
58 709.9	1.7	7.86	7.30	58 737	$4d_{5/2}9d$
58 856.2	10.0	8.20	7.58	58 829	$4d_{3/2}10d$
NO	—	—	—	59 066	$5p6p\,{}^3P_0$
59 258.8	5.5	9.45	8.52	59 280	$4d_{5/2}10d$
NO	—	—	—	59 323	$4d_{3/2}11d$
59 505.0	1.5	10.57	9.32	59 511	$4d_{3/2}12d$
59 556.5	1.0 B	10.85	9.51	59 569	$4d_{5/2}11d$
59 666.1	1.0	11.55	9.98	59 672	$4d_{3/2}13d$
59 777.1	1.0	12.42	10.51	59 780	$4d_{5/2}12d$
59 791.5	1.2 B	12.55	10.60	59 796	$4d_{3/2}14d$
59 889.6	1.5 B	13.54	11.17	59 892	$4d_{3/2}15d$
59 941.2	2.0	14.17	11.52	59 944	$4d_{5/2}13d$
59 969.1	0.5	14.54	11.72	59 971	$4d_{3/2}16d$
60 033.5	0.6	15.54	12.22	60 034.9	$4d_{3/2}17d$
60 067.9	1.3	16.16	12.52	60 070.0	$4d_{5/2}14d$
60 086.8	0.3	16.54	12.69	60 088.0	$4d_{3/2}18d$
60 131.2	0.5	17.54	13.12	60 132.1	$4d_{3/2}19d$
60 167.4	1.2	18.50	13.51	60 168.3	$4d_{5/2}15d$‡
60 177.2	0.4 B	18.79	13.62	60 170.2	$4d_{3/2}20d$‡
60 200.5	0.2	19.53	13.90	60 201.1	$4d_{3/2}21d$
60 227.6	0.4	20.5	14.24	60 228.3	$4d_{3/2}22d$
60 247.4	0.7	21.35	14.51	60 248.6	$4d_{5/2}16d$
60 251.4	0.4	21.53	14.57	60 251.9	$4d_{3/2}23d$
60 271.9	0.3	22.53	14.87	60 272.3	$4d_{3/2}24d$
60 289.9	0.3	23.53	15.14	60 290.2	$4d_{3/2}25d$
60 305.7	0.25	24.53	15.40	60 306.0	$4d_{3/2}26d$
60 312.4	0.65	24.99	15.51	60 313.3	$4d_{5/2}17d$
60 319.7	0.25	25.53	15.64	60 320.0	$4d_{3/2}27d$
60 332.0	0.25	26.51	15.86	60 332.4	$4d_{3/2}28d$
60 343.2	0.25	27.52	16.07	60 343.5	$4d_{3/2}29d$
60 353.2	0.2	28.52	16.26	60 353.4	$4d_{3/2}30d$
60 362.2	0.25	29.52	16.44	60 362.4	$4d_{3/2}31d$
60 366.0	0.65	29.98	16.51	60 366.7	$4d_{5/2}18d$
60 370.3	0.2	30.52	16.60	60 370.5	$4d_{3/2}32d$
60 377.7	0.25	31.53	16.76	60 377.9	$4d_{3/2}33d$
60 384.4	0.2	32.53	16.90	60 384.5	$4d_{3/2}34d$
60 390.6	0.25	33.55	17.04	60 390.6	$4d_{3/2}35d$
60 396.0	0.3	34.52	17.17	60 396.1	$4d_{3/2}36d$
60 401.2	0.2	35.54	17.29	60 401.2	$4d_{3/2}37d$
60 405.8	0.25	36.52	17.40	60 405.9	$4d_{3/2}38d$

Table 1. (continued)

$E_{expt.}$ (cm^{-1})	Width (cm^{-1})	$\nu d_{3/2}$	$\nu d_{5/2}$	$E_{theor.}$ (cm^{-1})	Label
60 410.2	0.25	37.53	17.50	60 410.2	$4d_{3/2}39d$
60 410.7	0.4	37.66	17.51	60 411.2	$4d_{5/2}19d$
60 414.2	0.3	38.54	17.60	60 414.2	$4d_{3/2}40d$
60 417.8	0.2	39.51	17.69	60 417.9	$4d_{3/2}41d$
60 421.3	0.2	40.53	17.78	60 421.2	$4d_{3/2}42d$
60 424.4	0.2	41.51	17.86	60 424.5	$4d_{3/2}43d$
60 427.5	0.2	42.56	17.94	60 427.5	$4d_{3/2}44d$
60 430.2	0.25	43.54	18.01	60 430.2	$4d_{3/2}45d$
60 432.8	0.2	44.55	18.08	60 432.8	$4d_{3/2}46d$
60 435.2	0.25	45.55	18.15	60 435.2	$4d_{3/2}47d$
60 437.5	0.2	46.57	18.21	60 437.4	$4d_{3/2}48d$
60 439.6	0.2	47.57	18.27	60 439.5	$4d_{3/2}49d$
60 441.6	0.2	48.59	18.32	60 441.5	$4d_{3/2}50d$
60 443.4	0.2	49.55	18.37	60 443.4	$4d_{3/2}51d$
60 445.2	0.2	50.58	18.43	60 445.1	$4d_{3/2}52d$
60 446.8	0.2	51.55	18.47	60 446.8	$4d_{3/2}53d$
60 447.9	0.2	52.25	18.50	60 448.3	$4d_{3/2}54d$‡
60 448.3	0.5	52.52	18.51	60 448.7	$4d_{5/2}20d$‡
60 449.8	0.2	53.54	18.56	60 449.8	$4d_{3/2}55d$
60 451.3	0.2	54.62	18.60	60 451.2	$4d_{3/2}56d$
60 452.6	0.2	55.61	18.64	60 452.5	$4d_{3/2}57d$
60 453.8	0.2	56.57	18.68	60 453.8	$4d_{3/2}58d$
60 455.0	0.2	57.59	18.71	60 455.0	$4d_{3/2}59d$
60 456.1	0.2	58.57	18.74	60 456.1	$4d_{3/2}60d$
60 457.3	0.2	59.70	18.78	60 457.1	$4d_{3/2}61d$
60 458.1	0.2	60.49	18.80	60 458.2	$4d_{3/2}62d$
60 459.2	0.2	61.63	18.84	60 459.1	$4d_{3/2}63d$
60 460.0	0.2	62.50	18.86	60 460.0	$4d_{3/2}64d$
60 460.9	0.2	63.53	18.89	60 460.9	$4d_{3/2}65d$
60 461.7	0.2	64.48	18.91	60 461.8	$4d_{3/2}66d$
60 480.0	0.6	116.47	19.51		$4d_{5/2}21d$
60 507.7	0.6		20.52		$4d_{5/2}22d$
60 531.3	0.6		21.51		$4d_{5/2}23d$
60 551.9	0.6		22.51		$4d_{5/2}24d$
60 570.0	0.4		23.52		$4d_{5/2}25d$
60 585.9	0.3		24.52		$4d_{5/2}26d$
60 600.0	0.3		25.52		$4d_{5/2}27d$
60 612.5	0.4		26.53		$4d_{5/2}28d$
60 623.5	0.4		27.52		$4d_{5/2}29d$
60 633.5	0.4		28.52		$4d_{5/2}30d$
60 642.5	0.4		29.52		$4d_{5/2}31d$
60 650.6	0.4		30.52		$4d_{5/2}32d$
60 658.0	0.4		31.53		$4d_{5/2}33d$
60 664.6	0.35		32.52		$4d_{5/2}34d$
60 670.8	0.3		33.52		$4d_{5/2}35d$
60 676.4	0.3		34.53		$4d_{5/2}36d$
60 681.5	0.25		35.52		$4d_{5/2}37d$
60 686.2	0.3		36.53		$4d_{5/2}38d$
60 690.5	0.3		37.51		$4d_{5/2}39d$
60 694.5	0.2		38.52		$4d_{5/2}40d$
60 698.2	0.25		39.51		$4d_{5/2}41d$
60 701.6	0.2		40.53		$4d_{5/2}42d$

Table 1. (continued)

$E_{expt.}$ (cm^{-1})	Width (cm^{-1})	$\nu d_{3/2}$	$\nu d_{5/2}$	$E_{theor.}$ (cm^{-1})	Label
60 704.8	0.2		41.53		$4d_{5/2}43d$
60 707.8	0.25		42.54		$4d_{5/2}44d$
60 710.5	0.25		43.53		$4d_{5/2}45d$
60 713.1	0.2		44.54		$4d_{5/2}46d$
60 715.5	0.2		45.54		$4d_{5/2}47d$
60 717.8	0.2		46.55		$4d_{5/2}48d$
60 719.9	0.2		47.53		$4d_{5/2}49d$
60 721.8	0.2		48.53		$4d_{5/2}50d$
60 723.7	0.2		49.53		$4d_{5/2}51d$
60 725.5	0.2		50.53		$4d_{5/2}52d$
60 727.1	0.2		51.55		$4d_{5/2}53d$
60 728.6	0.2		52.51		$4d_{5/2}54d$
60 730.1	0.2		53.51		$4d_{5/2}55d$
60 731.5	0.2		54.54		$4d_{5/2}56d$
60 732.9	0.2		55.54		$4d_{5/2}57d$
60 734.1	0.2		56.51		$4d_{5/2}58d$
60 735.2	0.2		57.49		$4d_{5/2}59d$
60 736.4	0.2		58.53		$4d_{5/2}60d$
60 737.5	0.2		59.55		$4d_{5/2}61d$
60 738.4	0.2		60.49		$4d_{5/2}62d$
60 739.5	0.2		61.56		$4d_{5/2}63d$
60 740.3	0.2		62.49		$4d_{5/2}64d$

the energy E. Using the jj-LS geometric frame transformation, the LS-coupled reaction matrices are recoupled into a larger jj-coupled reaction matrix $K(E)$ referring to five dissociation channels ($5s_{1/2}\varepsilon s_{1/2}$, $4d_{3/2}nd_{3/2}$, $4d_{5/2}nd_{5/2}$, $5p_{1/2}np_{1/2}$ and $5p_{3/2}np_{3/2}$). The calculation of observable quantities from the short-range matrix $K(E)$ proceeds by standard MQDT techniques. The only place at which fine structure enters the calculation is this last stage where experimental j-dependent thresholds are used in the MQDT calculations.

Two complementary calculations have been done: the first one is restricted to calculating only the positions of the autoionizing lines while the second concerns both the positions and profiles of the resonances.

5.2. Energy positions of the autoionizing levels

The structure of the $J=0^e$ autoionizing spectrum reflects the mixing of the $5s\varepsilon s$ continuum with the doubly excited states associated with the four $4dnd$ and $5pnp$ closed channels. As previously explained (Fano and Rau 1986, Lecomte 1987, Kompitsas *et al* 1990), the complete $K(E)$ reaction matrix referring to closed and open channels can be contracted to give an effective $K_{eff}(E)$ matrix restricted to closed channels only. Using this matrix, MQDT techniques adapted to bound spectra can be used to calculate the positions of resonant states as well as to analyse channel mixing. This results in the Lu-Fano plot shown in figure 8, which allows comparison with the present experimental results. The theoretical energy values are presented in table 1.

All the observed resonances can be associated unambiguously with a theoretical energy and the departures of the experimental points from the theoretical curve are small. The underlying procedure used is adequate to locate each resonance position

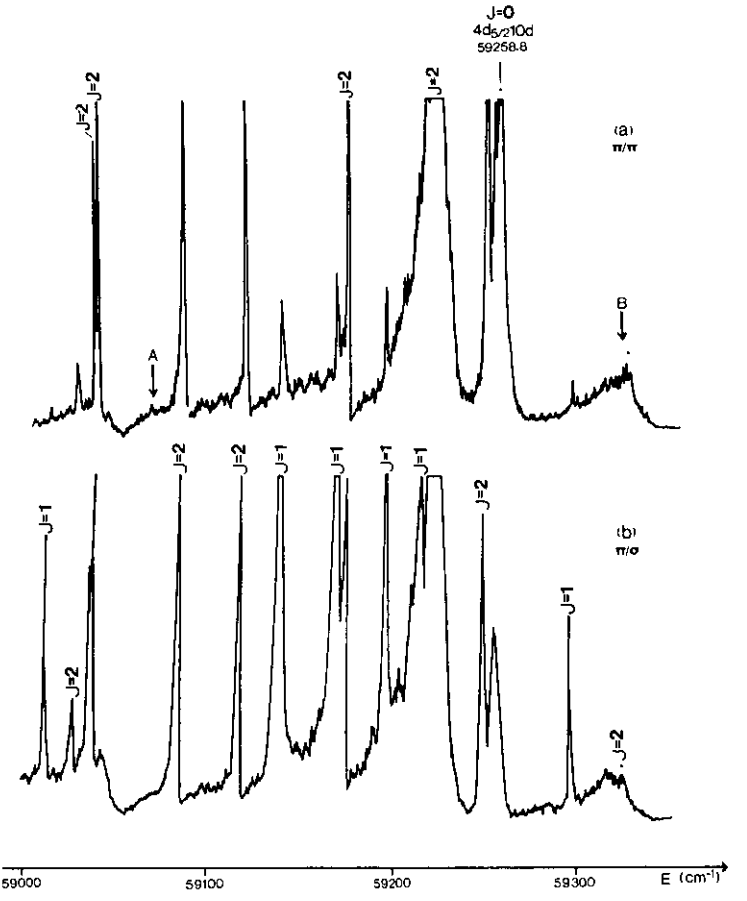

Figure 6. Two-step excitation spectra. In the $\pi\pi$ spectrum (a), the arrows A and B indicate the predicted locations of the unobserved $5p6p\ ^3P_0$ perturber and $4d_{3/2}11d$ $J=0$ series member by comparison with the $\pi\sigma$ spectrum (b).

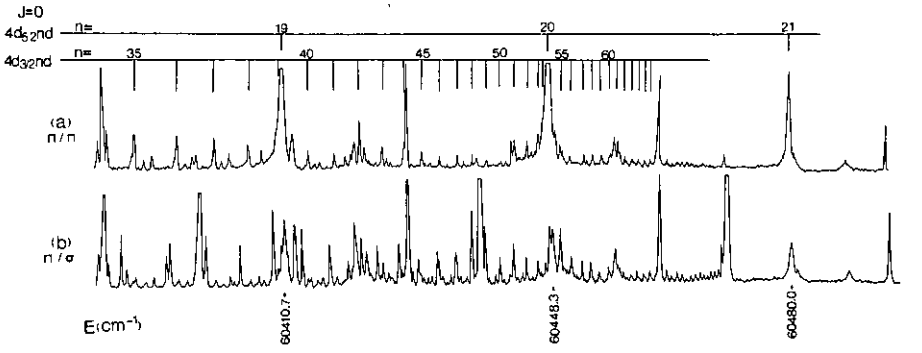

Figure 7. Two-step $\pi\pi$ (a) and $\pi\sigma$ (b) excitation spectra close to the $4d_{3/2}$ threshold. Note how the $5d_{5/2}20d$ level perturbs the $4d_{3/2}54d$ and $d_{3/2}55d$ $J=0$ series members shifting them to lower and higher energies respectively.

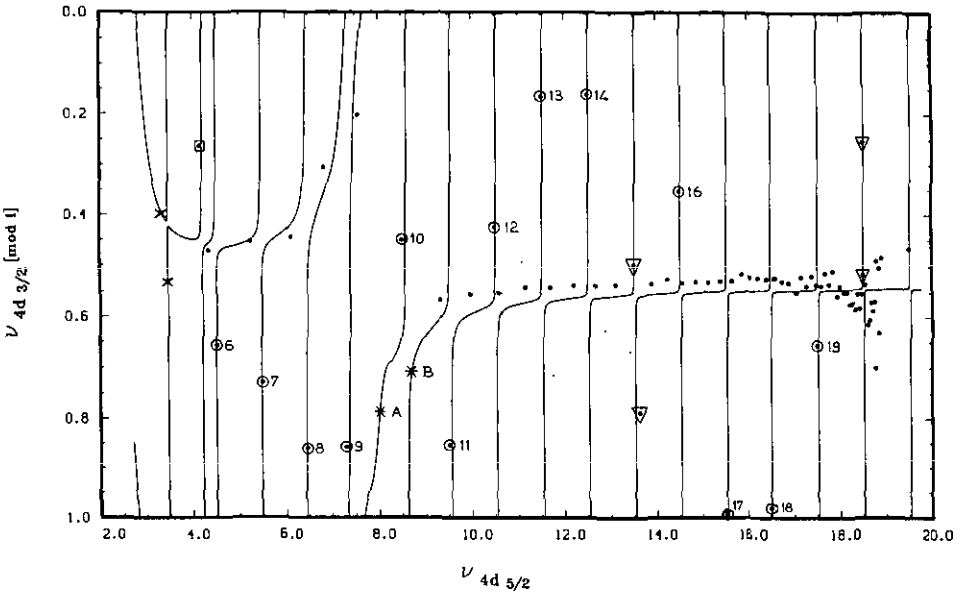

Figure 8. Lu–Fano plot of the energy positions of the $J = 0^e$ autoionizing levels of Sr. Experimental data: ⊙, $4d_{5/2}nd_{5/2}$; ●, $4d_{3/2}nd_{3/2}$; ▽, see text; ⊡, $5p^2\,{}^1S_0$. The full line corresponds to the R-matrix result. The asterisks refer to the energy positions predicted for the unobserved resonances (for A and B see figure 6).

with an error comparable to its autoionization width. For high-lying levels the difference between the observed and calculated energies is of the same order as the autoionization width (or experimental uncertainty). As evident from table 1, the largest deviations between experimental and theoretical energies occur in the low energy range.

Two different regions of the $J = 0^e$ autoionizing spectrum below the $4d_{3/2}$ threshold can be considered. In the high-energy range, for $E > 59\,700\ \text{cm}^{-1}$ ($\nu_{5/2} > 10$) the observed structures can be described by a two-channel model relevant to describe the $4d_{3/2}nd$ series perturbed periodically by the $4d_{5/2}nd$ levels. In this zone, almost pure *jj* coupling holds for the levels, the mixing between both 4d*n*d channels being generally very weak, as illustrated by the very small gaps between the branches of the Lu–Fano plot associated with the $4d_{3/2}nd$ and $4d_{5/2}nd$ series. However near $\nu_{5/2} = 13.5$ and 18.5 levels of both 4d*n*d series are very close and thus they strongly interact. As indicated in table 1 and figure 11, there is difficulty in labelling these levels unambiguously. In the lower energy range, the situation is obviously more complex. There, the MQDT parameters acquire a strong energy dependence and both 4d*n*d series are affected by the presence of two perturbers located near $\nu_{5/2} = 4$ and 8. The lower perturber corresponds to the broad autoionizing profile observed at $54\,451\ \text{cm}^{-1}$. Our MQDT analysis shows that this level has a p^2 component twice as large as the d^2 one and thus this level supports the $5p^2\,{}^1S_0$ label; the low-lying bound level at $37\,160\ \text{cm}^{-1}$ labelled $5p^2\,{}^1S_0$ in Moore's table has to be identified with the $4d^2\,{}^1S_0$ level. However it must be kept in mind that the single-particle label is not appropriate for such strongly mixed nl^2 levels. The present study is in agreement with the results of the previous R-matrix calculation done in *LS* coupling (Aymar *et al* 1987).

The second perturber identified by our theoretical analysis with the $5p6p\,{}^3P_0$ level has not been observed. However its effect on the positions of neighbouring 4d*n*d levels

is quite visible on the Lu-Fano plot of figure 8. Moreover it also perturbs the oscillator strengths of the 4d5p $^1P_1 \rightarrow 4dnd$ $J=0$ transitions; in particular the $4d_{3/2}11d$ $J=0$ level predicted to lie near 59 323 cm^{-1} has not been observed (arrow B on figure 6). The 5p6p $^3P_0$ perturber is mixed with several 4d*n*d $J=0$ levels and the theoretical level identified in table 1 as the 5p6p $^3P_0$ level corresponds to the largest $5p_{1/2}np$ component.

5.3. Profiles of the autoionizing levels

The high energy position of the 4d5p $^1P_1$ level used as the starting level for the second step in this experiment made it difficult for us to calculate the photoionization spectrum out of this level by using the procedure employed for photoionization out of the ground state (Aymar 1987) or a low-lying level (Kompitsas *et al* 1990). This procedure in fact supposes that the starting level should be contained within the reaction volume and it is clear that the 4d5p $^1P_1$ level cannot be correctly described within a reaction volume of 20 au.

R-matrix calculations with a much larger reaction volume, not being a trivial extension of this work, have not yet been done. To get some information on the widths of the autoionizing levels we have considered rather the 5s6p $^1P_1 \rightarrow J=0^e$ photoionization process. The determination of the wavefunction of the 5s6p $^1P_1$ level has been obtained by standard diagonalization within the reaction volume of radius $r_0 = 20$ au. Calculation of the dipole matrix elements connecting the 5s6p $^1P_1$ level to the *R*-matrix eigenstates for the $^1S_0^e$ symmetries allows the calculation of photoionization cross sections.

Figures 9, 10 and 11 display the 5s6p $^1P_1 \rightarrow J=0^e$ photoionization cross sections in different energy ranges. The vertical bars refer to the positions of the resonant states as observed in the present study from the 5s7p $^1P_1$ or 4d5p $^1P_1$ level. Because the starting level used in the calculation differs from that used in the experiment, no quantitative comparisons can be made on the intensities and profiles of the resonances.

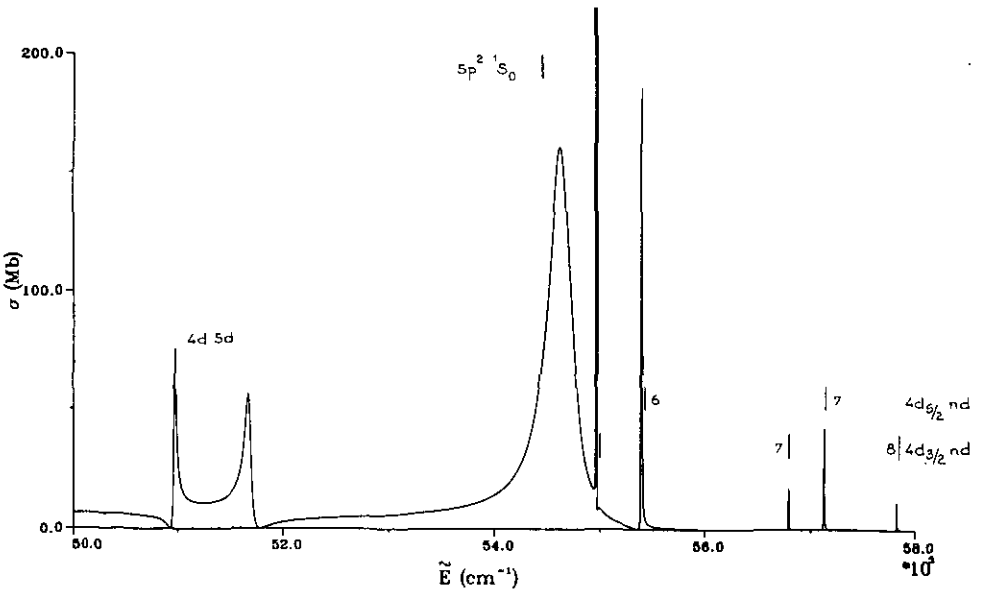

Figure 9. Theoretical 5s6p $^1P_1 \rightarrow J=0^e$ photoionization spectrum in the 50 000–58 000 cm^{-1} energy range. The vertical bars refer to the positions of the observed resonances.

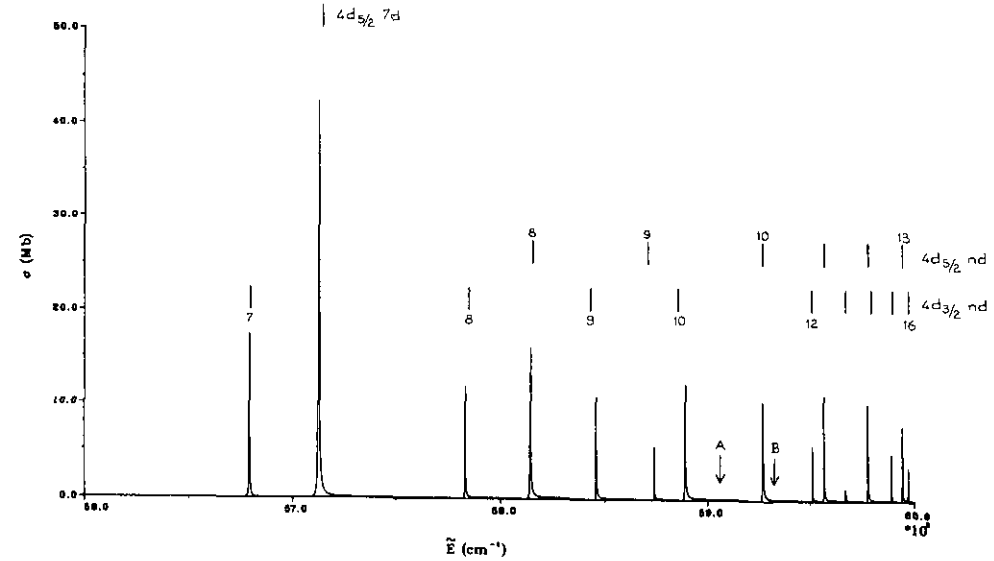

Figure 10. Same as in figure 9, in the 56 000–60 000 cm^{-1} energy range. The vertical arrows correspond to the theoretical energy positions of the unobserved resonances $5p6p\ ^3P_0$ (A) and $4d_{3/2}11d_{3/2}$ (B) (see figure 6).

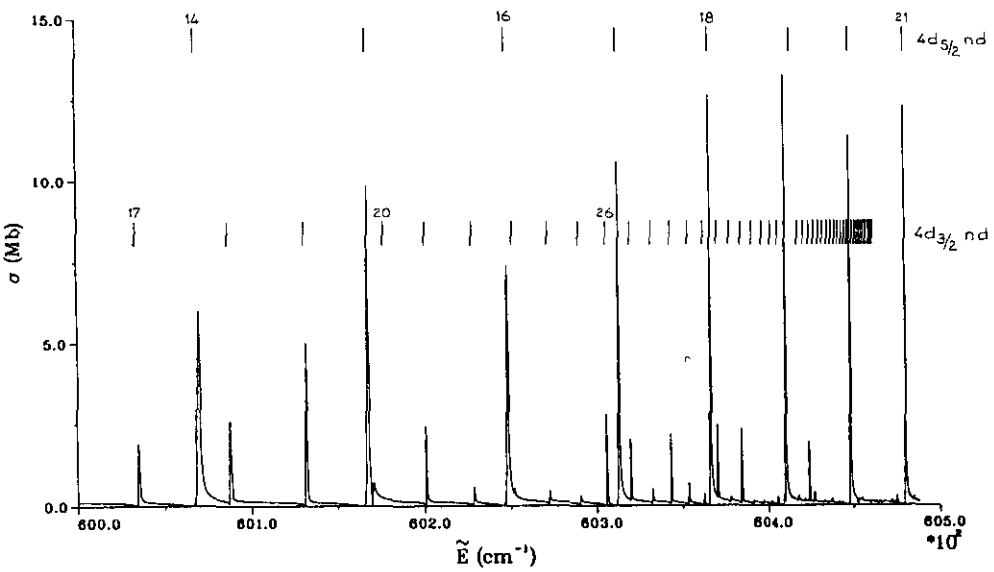

Figure 11. Same as in figure 9, in the energy range from 60 000 cm^{-1} to the $4d_{3/2}$ limit.

Figure 9 deals with the lower energy range where the $5p^2\ ^1S_0$ resonance lies and whose characteristics (position and width) are in qualitative agreement with the experiment. All the 4d*n*d resonances are narrow except those associated with the 4d5d levels. The two levels associated with the 4d5d levels are large and overlapping and thus the shapes of these resonances are expected to strongly depend on the starting level used to excite them; however the fact that they are relatively broad may perhaps explain why these levels were not observed in the direct two-photon experiment.

The calculated $5s6p\ ^1P_1 \rightarrow J = 0^e$ photoionization spectrum in the intermediate energy range (56 000–60 000 cm^{-1}) is displayed in figure 10. In this energy range two resonant states associated with the $5p6p\ ^3P_0$ and $4d_{3/2}11d$ levels respectively have not been observed from the $4d5p\ ^1P_1$ level (figure 6). The predicted positions for these levels are indicated in figure 10 by vertical arrows. It is interesting to note that these levels also do not appear in the $5s6p\ ^1P_1 \rightarrow J = 0^e$ spectrum. The irregular behaviour of the intensities reflects mainly the presence of the perturber.

The calculated photoionization spectrum in the energy range just below the $4d_{3/2}$ threshold is shown in figure 11. This figure illustrates that the $4d_{5/2}nd$ lines are much stronger than the $4d_{3/2}nd$ lines (see figure 7). In this energy range as well as above the $4d_{3/2}$ threshold, the $4d_{5/2}nd$ $J = 0$ series is characterized by an almost constant quantum defect of 1.49.

6. Conclusion

In this work the energy positions of the $4dnd$ $J = 0$ series are measured below the 4d threshold. A further important result of our measurements is the identification of the $5p^2\ ^1S_0$ level as a broad autoionizing resonance at 54 451 cm^{-1}. We applied a two-step excitation process via an appropriate $^1P_1$ intermediate level. Among the final J values of the observed resonances being 0, 1 or 2, we could identify the $J = 0$ ones by simply comparing $\pi\pi$ and $\pi\sigma$ spectra in the same energy range, since the $J = 0$ resonances appear only in the $\pi\pi$ spectra and the $J = 1$ resonances only in the $\pi\sigma$ spectra. This method appeared to give reliable results even in such complicated spectra as ours. The theoretical calculations based on the combined eigenchannel R-matrix and MQDT methods have described the energies of the $4dnd$ levels successfully. In particular they show that the $5p^2\ ^1S_0$ state is a strong perturber of the $4dnd$ $J = 0$ series and they predict the $5p6p\ ^3P_0$ perturber which could not be observed experimentally from the intermediate level used here. The calculation of the $5s6p\ ^1P_1 \rightarrow J = 0^e$ photoionization spectrum allows us to interpret qualitatively some observations obtained for the $4d5p\ ^1P_1 \rightarrow J = 0^e$ spectrum.

The identification of the $5p^2\ ^1S_0$ resonance in the autoionizing region of the spectrum completes the data for the positions of the lowest $ml^2\ ^1S_0$ levels of the alkaline earths. In Be (Clark *et al* 1985), Mg (Bonanno *et al* 1986), Sr (this work) and Ba (Aymar *et al* 1982) the lowest $mp^2\ ^1S_0$ level corresponds to a broad autoionizing resonance. In Sr and Ba the $mp^2\ ^1S_0$ level strongly interacts with the $(m-1)d^2\ ^1S_0$ bound level. In Ca (Armstrong *et al* 1977) the $4p^2\ ^1S_0$ label was given to a low lying bound level but the $3d^2\ ^1S_0$ level, expected to lie above the first ionization limit, is unknown. It seems that the positions of these broad, low-lying autoionizing levels play an important role in atomic spectroscopy, since they strongly perturb Rydberg series. Moreover we note that they can be used as first-step intermediates in multistep excitation processes towards higher lying doubly-excited states of similar type. The latter are interesting cases for the study of the electron correlations.

Acknowledgments

We thank Professor C A Nicolaides, Director of the Theoretical and Physical Chemistry Institute, for financial support and for reading the manuscript. This work has been

supported in part by the Centre National de la Recherche Scientifique and the National Hellenic Research Foundation in the framework of an Exchange Visitor Program.

References

Armstrong J A, Esherick P and Wynne J J 1977 *Phys. Rev.* A **15** 180
Aspect A, Bauche J, Fonseca A L A, Grangier P and Roger G 1984 *J. Phys. B: At. Mol. Phys.* **17** 1761
Aymar M 1987 *J. Phys. B: At. Mol. Phys.* **20** 6507
—— 1990 *J. Phys. B: At. Mol. Opt. Phys.* **23** 2697
Aymar M, Camus P and El Himdy A 1982 *J. Phys. B: At. Mol. Phys.* **15** L759
Aymar M and Lecomte J M 1989 *J. Phys. B: At. Mol. Opt. Phys.* **22** 223
Aymar M, Luc-Koenig E and Watanabe S 1987 *J. Phys. B: At. Mol. Phys.* **20** 4325
Baig M A and Connerade J P 1984 *J. Phys. B: At. Mol. Phys.* **17** L271
Bonanno R E, Clark C W and Lucatorto T B 1986 *Phys. Rev.* A **34** 2082
Brown C M, Longmire M S and Ginter M L 1983 *J. Opt. Soc. Am.* B **73** 985
Camus P, Kompitsas M, Cohen S, Nicolaides C, Aymar M, Crance M and Pillet P 1989 *J. Phys. B: At. Mol. Opt. Phys.* **22** 445–58
Clark C W, Fassett J D, Lucatorto T B and Moore L J 1985 *J. Opt. Soc. Am.* **2** 891
Connerade J P, Baig M A, Garton W R S and Newsom G H 1980 *Proc. R. Soc.* A **371** 295–307
Esherick P 1977 *Phys. Rev.* A **15** 1920
Fano U and Rau A R P 1986 *Atomic Collisions and Spectra* (New York: Academic)
Froese-Fischer C and Hansen J E 1981 *Phys. Rev.* A **24** 631
Garton W R S and Codling K 1968 *J. Phys. B: At. Mol. Phys.* 1 106
Greene C H 1985 *Phys. Rev.* A **32** 1880
Hudson R D, Carter V L and Young P A 1969 *Phys. Rev.* **180** 77
Jonsson G, Levison C, Persson A and Wahlstrom C G 1984 *Z. Phys.* A **316** 255
Kim L and Greene C H 1987 *Phys. Rev.* A **36** 4272
—— 1988 *Phys. Rev.* A **38** 2361
Kompitsas M, Cohen S, Nicolaides C A, Robaux O, Aymar M and Camus P 1990 *J. Phys. B: At. Mol. Opt. Phys.* **23** 2247
Lecomte J M 1987 *J. Phys. B: At. Mol. Phys.* **20** 3645
Lu K T 1977 *Proc. R. Soc.* A **353** 431
Moore C E 1971 *Atomic Energy Levels* NBS 35, Vol 11 (Washington, DC: US Govt Printing Office)
Newsom G H, O'Connor S and Learner R C M 1973 *J. Phys. B: At. Mol. Phys.* **6** 2162
Seaton M J 1983 *Rep. Prog. Phys.* **46** 167
Vaeck N, Godefroid M and Hansen J E 1988 *Phys. Rev.* A **38** 2830
Xu E Y, Zhu Y, Mullins O C and Gallagher T F 1986 *Phys. Rev.* A **33** 2401
—— 1987 *Phys. Rev.* A **35** 1138
Zhu Y, Xu E Y and Gallagher T F 1987 *Phys. Rev.* A **36** 3751